

A tunable photonic band gap resonator for axion dark matter searches

Samantha M. Lewis,^{1,2,*} Dillon T. Goulart,² Mirelys Carcana Barbosa,^{2,†} Alexander F. Leder,^{2,3} Aarav M. Sindhwad,² Isabella Urdinaran,² and Karl van Bibber²

¹*Department of Physics and Astronomy, Wellesley College, Wellesley, Massachusetts 02481, USA*

²*Department of Nuclear Engineering, University of California, Berkeley, Berkeley, California 94720, USA*

³*Physics Division, Los Alamos National Laboratory, Los Alamos, New Mexico 87545, USA*

(Dated: August 8, 2024)

Axions are a well-motivated dark matter candidate particle. Haloscopes aim to detect axions in the galactic halo by measuring the photon signal resulting from axions interacting with a strong magnetic field. Existing haloscopes are primarily targeting axion masses which produce microwave-range photons and rely on microwave resonators to enhance the signal power. Only a limited subset of resonator modes are useful for this process, and current cylindrical-style cavities suffer from mode mixing and crowding from other fundamental modes. The majority of these modes can be eliminated by using photonic band gap (PBG) resonators. The band gap behavior of these structures allows for a resonator with mode selectivity based on frequency. We present results from the first tunable PBG resonator, a proof-of-concept design with a footprint compatible with axion haloscopes. We have thoroughly characterized the tuning range of two versions of the structure and report the successful confinement of the operating TM_{010} mode and the elimination of all TE modes within the tuning range.

I. INTRODUCTION

The axion is a hypothetical particle which arises from a proposed solution to the Strong CP problem [1–4]. Its properties also make the axion a well-motivated dark matter candidate particle [5, 6]. One of the leading techniques to search for axions attempts to measure the axion conversion to a photon in the presence of an applied magnetic field [7]. In this process, the resulting photon carries the full energy of the axion. In the case of experiments searching for virialized axions in the galactic dark matter halo (called ‘haloscopes’), the photon frequency is related to the axion mass as

$$h\nu = m_a c^2 \left[1 + \frac{1}{2} \mathcal{O}(\beta^2) \right], \quad (1)$$

where ν is the photon frequency, h is Planck’s constant, m_a is the axion mass, c is the speed of light, and $\beta \approx 10^{-3}$ is the galactic virial velocity [8].

Traditional axion haloscopes combine a high field superconducting magnet, a dilution refrigerator, a low noise readout system, and a tunable electromagnetic cavity to search for the converted photon signal. The goal is to tune the frequency of a cavity mode to match the frequency of the converted photon, resulting in resonant enhancement of the signal. The efficiency of this conversion is highest when the cavity electric field is aligned with the applied magnetic field, quantified by a mode-dependent form factor $C_{nm\ell}$. For experiments using a solenoid with a uniform magnetic field along \hat{z} , the form

factor is

$$C_{nm\ell} = \frac{\left(\int d^3\mathbf{x} \hat{\mathbf{z}} \cdot \mathbf{E}_{nm\ell}(\mathbf{x}) \right)^2}{V \int d^3\mathbf{x} \epsilon(\mathbf{x}) |\mathbf{E}_{nm\ell}|^2} \quad (2)$$

where V is the cavity interior volume, ϵ is the relative permittivity of any material inside the cavity, and $\mathbf{E}_{nm\ell}$ is the electric field of the mode specified by indices n , m , and ℓ . In the cylindrical cavities used in many axion haloscopes, the lowest order transverse magnetic mode TM_{010} has the highest possible form factor with an E field purely along the z axis, fully aligned with the magnetic field of the external solenoid. The overall cavity performance contributes to the signal power as

$$P \propto V Q_L C_{nm\ell}, \quad (3)$$

where Q_L is the loaded quality factor of the cavity mode.

Both the mass of the axion and the coupling strength of the axion to photon conversion $g_{a\gamma\gamma}$ are unknown. Various astrophysical constraints limit the upper bound of QCD cold dark matter axion masses to roughly 15 meV or 50 meV, depending on the model [9–11]. The possible range covers many orders of magnitude in mass and therefore frequency. As a result, a variety of experiments are being performed and built around the world to cover this wide range, with search frequencies down to the kHz scale and up the THz scale [10]. In the microwave frequency range, haloscopes use tunable cavities in order to search over a range of axion masses in each experimental run. The expected signal power is extremely small, so experiments must integrate for some time at each frequency point to achieve sensitivities corresponding to the model bands of interest for the QCD axion.

In currently operating haloscope cavities, frequency tuning is achieved using one or more cylindrical tuning rods which can be rotated, changing the frequency of all transverse magnetic (TM) modes. This method

* sl128@wellesley.edu

† Now at Brown University

of tuning does not appreciably tune transverse electric (TE) and transverse electromagnetic (TEM) modes. For a standard cylindrical cavity with a metallic tuning rod, all possible TE, TM, and TEM modes are supported. As the operating TM_{010} mode is tuned, it crosses the stationary TE and TEM modes. By definition, TE and TEM modes have no significant E_z component and therefore have C_{nml} values of zero. As the TM_{010} approaches a stationary mode, the two modes mix, reducing the E_z component of the field and by extension the form factor of the hybridized mode. The reduction in form factor is significant over a range of frequencies around the stationary mode, making it unfeasible to search for axions in that range [12]. Such mode crossings are one cause for the gaps in published haloscope exclusion limits [13–15]. Filling in these gaps requires time-intensive mechanical reconfiguration of the cavity and more run time at the affected frequency range.

Eliminating unwanted stationary modes would speed up axion searches by making more of the cavity tuning range usable in a given experiment, removing the need for cavity reconfiguration. Many of the cavity innovations of interest for next generation axion searches also face challenges with mode crossings or mode mixing [16, 17]. The mode crossing problem also limits the feasibility of using higher order TM modes for searches, or longer cylindrical cavities, where in both cases the density of TE modes is higher. Mode selectivity can be achieved using advanced resonator techniques such as microwave photonic band gap (PBG) structures.

In this paper, we present results from a proof-of-concept tunable PBG resonator designed to be used in an axion haloscope. Section II describes the principle of PBG structures and outlines the tunable resonator design. Section III describes the methods used to characterize the device performance. Sections IV and V detail the results of two test cases. The conclusions and future work are summarized in Section VI.

II. PHOTONIC BAND GAP STRUCTURE DESIGN

A PBG consists of a periodic array of elements which give rise to a photonic band structure. For some configurations, there are band gaps in which photons of certain frequencies cannot propagate through the lattice [18]. These band gaps are analogous to electronic band gaps in materials [19]. One type of 2D PBG lattice in the microwave range can be made using metallic cylindrical rods. Figure 1 shows the geometry of a triangular 2D lattice. The band structure is determined by the rod radius a and the center-to-center rod spacing b [20, 21].

A defect can be created in a PBG lattice to confine a mode with a frequency within the band gap. Confinement occurs even without an overall outer reflecting boundary, so any excited modes with frequencies outside of the band gaps can propagate out of the structure.

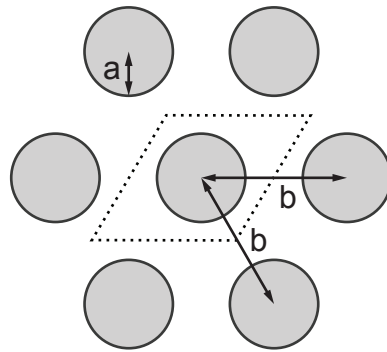


FIG. 1. Example 2D arrangement based on a triangular lattice, showing the rod spacing b and radius a . The dashed line indicates the unit cell.

While PBG theory is based on an infinite lattice, experiments have shown as few as 3 rows of rods can give sufficient confinement of the desired mode [21]. Many 2D PBG structures have been successfully used to confine a variety of chosen TE and TM modes in waveguides and resonators [22–27].

A triangular, metallic PBG lattice has several large band gaps for TM modes, but very few band gaps for TE modes [20]. As a result, a variety of lattice configurations will support TM modes with no nearby TE modes, the ideal scenario for axion haloscopes.

The previously cited microwave PBG resonators and waveguides are all designed to operate at a single precise frequency. In order to use a PBG lattice as a resonator for an axion search, it must be possible to freely tune the mode confined in the defect over a wide frequency range without reintroducing TE modes. To test whether it is possible to break symmetry in the structure and maintain the band gap behavior, we designed a resonator for an axion haloscope using the same tuning method as current cavities: an off-axis, cylindrical tuning rod which tunes a TM_{010} -like mode. Design simulations were performed using both CST Microwave Studio [28] and Ansys HFSS [29]. The structure was designed to have $a/b = 0.43$ with $a = 0.125$ in, corresponding to a rod spacing of $b = 0.2907$ in. The height of the lattice between the endcaps is 10 in. A tuning with radius $r = 0.32$ in $\approx 1.1b$ gives a tuning range of roughly 7.352–9.343 GHz. The size of this tuning range is comparable to similar existing haloscope cavities.

Figure 2 shows a top-down view of the electric field in the lattice at three tuning positions and the corresponding simulated tuning curve of the TM_{010} -like mode. The simulated performance of this structure is comparable to that of existing copper cylindrical cavities, with room temperature Q_0 values of order 10^4 for copper rods and endcaps. The structure as designed supports TM modes and no TE modes within the tuning range. TEM modes are introduced due to the metal tuning rod. However, previous work has shown that TEM mode crossings, while undesirable, have a smaller frequency range over

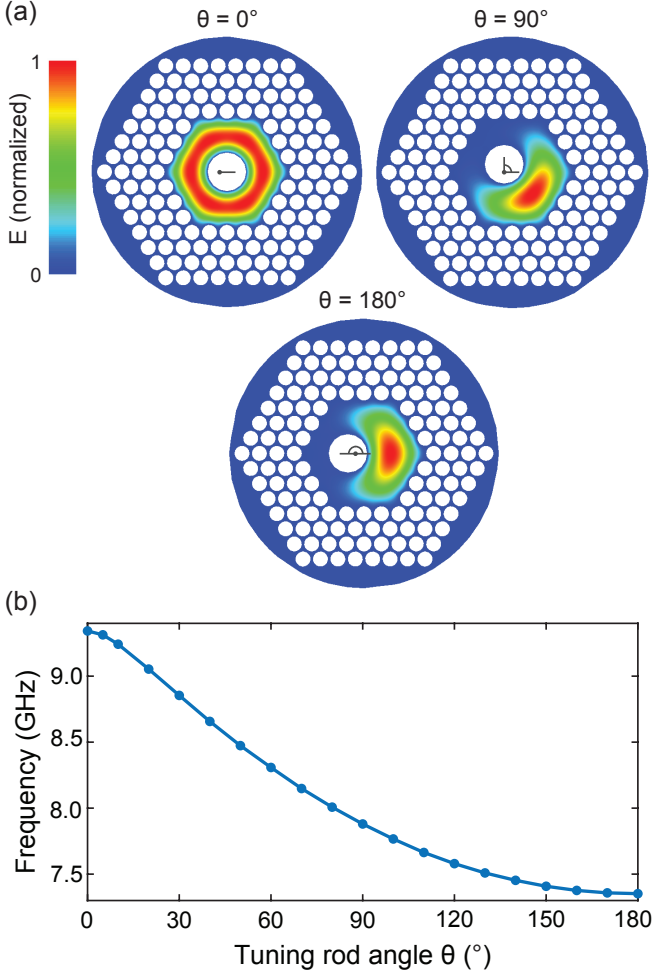


FIG. 2. (a) Normalized magnitude of the electric field in the structure at tuning rod angles of $\theta = 0^\circ$, 90° , and 180° . The HFSS simulation shown here includes a radiating boundary condition on the outer cylindrical surface. (b) Tuning curve generated from HFSS simulations of the structure including antenna coupling and the alignment grid. Simulations of 10° steps are shown, with an additional point at 5° to show the curvature of the tuning at the highest frequencies.

which they reduce the form factor, making them more tolerable [12].

The PBG structure was built using solid copper lattice rods, a copper tuning rod, and 1 in thick copper endcaps. Each PBG rod is press-fit into pockets in the endcaps. Six rods at the outer corners of the structure are tapped on both ends to bolt the structure together. The length of the tuning rod is 9.984 in, designed to leave 0.008 in gaps on either side of the tuning rod for rotation. A 1 mm thick PETG plastic 3D-printed alignment grid is used to hold the rods in place during assembly. This alignment grid was included in the simulation results presented and has minimal impact on the electrical performance.

III. MEASUREMENT GOALS AND METHODOLOGY

Our goal with this proof of concept structure was to determine whether the introduction of the tuning rod (breaking symmetry in the defect) affects the band gap behavior or causes the re-introduction of TE modes. While frequency tuning behavior can be determined solely from transmission measurements of the cavity, bead pull measurements are necessary to verify that the mode being tuned is the TM_{010} mode, study mode crossings, and ensure there is no unexpected mixing from any hard-to-see modes.

Bead pull measurements map out the field profile in one dimension by introducing a small perturbation that shifts the mode frequency by an amount proportional to the local electric field squared [30, 31]. An ideal TM_{010} mode has a constant electric field in the longitudinal direction, giving a constant frequency versus bead position. All TE and TEM modes have nodes in the longitudinal direction, resulting in oscillations of the frequency as a function of bead position. Figure 3 shows example bead pull measurements for a TM_{010} mode and a TE mode.

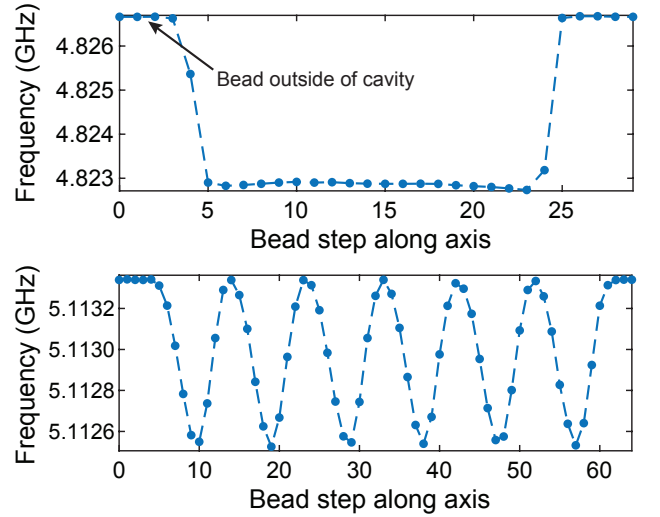


FIG. 3. Example bead pull measurements from two different cavities. In both cases, the frequency is constant at the unperturbed value when the bead is outside of the cavity. The top shows a near ideal TM_{010} , with a constant field along z resulting in a near constant perturbed frequency. This measurement was taken from an early, shorter prototype of the PBG with no tuning rod. The bottom shows an example TE mode from a standard cylindrical cavity, where the frequency returns to the unperturbed value at nodes in the E field.

The mode frequency is determined by measuring the peak in the transmission spectrum (S_{21}) using a vector network analyzer (VNA). Our test stand uses a Keysight E5071C ENA. We couple to the cavity using two adjustable coaxial probe antennas located at the top of the cavity. The rotation of the tuning rod and the bead line are controlled using Applied Motion Products stepper

motors. For our bead, we used a 1/8 inch diameter nylon sphere on monofilament nylon suture line. Further details on the bead pull test stand used can be found in Refs. [12, 32]. Photos of the PBG structure mounted on the test stand are shown in Fig. 4.

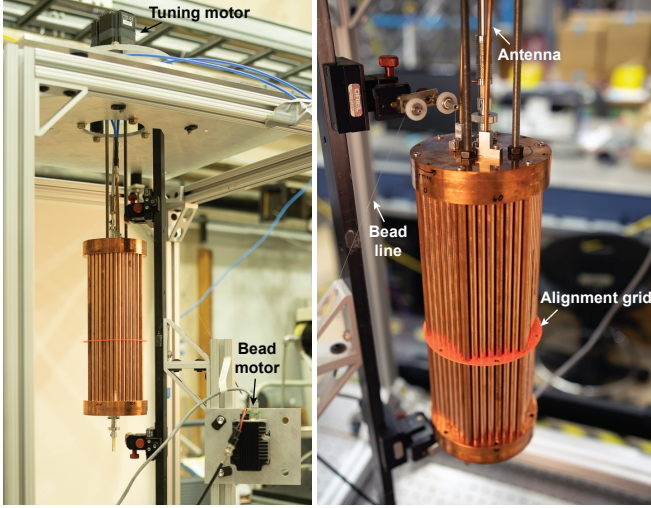


FIG. 4. The assembled PBG structure mounted on the bead pull test stand. The left photo shows both motors used in the measurements. The right photo provides a close up view showing the bead line, one variable coupling antenna, and the alignment grid.

To test the PBG performance and effectiveness at eliminating TE modes, we measured the TM_{010} mode profile at 1° steps in tuning rod angle throughout the entire tuning range. TE and TEM modes typically couple poorly to the antenna orientation used and may not be visible in a measured spectrum until they are mixing with a nearby TM mode. To ensure there were no unexpected TE modes that may be poorly confined with low Q values or limited coupling, we repeated the measurement procedure at several antenna couplings.

Vibrations of the bead line, cavity, or tuning rod can cause changes to the bead pull measurement. The test stand is built with vibration isolation between components, but additional wait times are occasionally needed for clean measurements. As part of this work, full automation of the bead pull test stand was developed, allowing for longer wait times and fine, repeatable steps in the tuning rod angle.

IV. FOUR ROW DESIGN RESULTS

The design tuning range of the four row structure was 7.352–9.343 GHz (Fig. 2). The measured TM_{010} mode range was slightly higher, from 7.428–9.409 GHz. There were a number of performance limitations in this prototype design. Most notably, the electrical contact between the PBG rods and endcaps was variable, resulting in lower than expected Q values at all frequencies. The

aspect ratio of the defect was also more extreme than typical haloscope cavities, resulting in difficulty coupling to the TM_{010} mode at some rod angles. This same limitation has been observed in other high aspect ratio cylindrical test cavities and is consistent with axial mode localization that occurs in these cases.

Together, these two factors limited the bead pull measurement quality at a small subset of rod angles. A plot showing the mode map for the four row design is shown in Figure 5, where these regions are visible. The TEM mode frequencies are based on the length of the cavity. In the measurement range, the expected TEM modes are the 13th, 14th, 15th, and 16th order modes at 7.67, 8.26, 8.85, and 9.44 GHz, respectively. The four expected TEM modes are visible on the mode map, especially at angles where they are mixing with a nearby TM mode. In other regions, the TEM modes are less visible due to coupling, as previously described. This limited visibility motivates the need for bead pull measurements at all rod angles to ensure there is truly no mixing. No unexpected modes were encountered, though the performance cannot be sufficiently characterized in the regions of the tuning range where the coupling and Q value were especially limited.

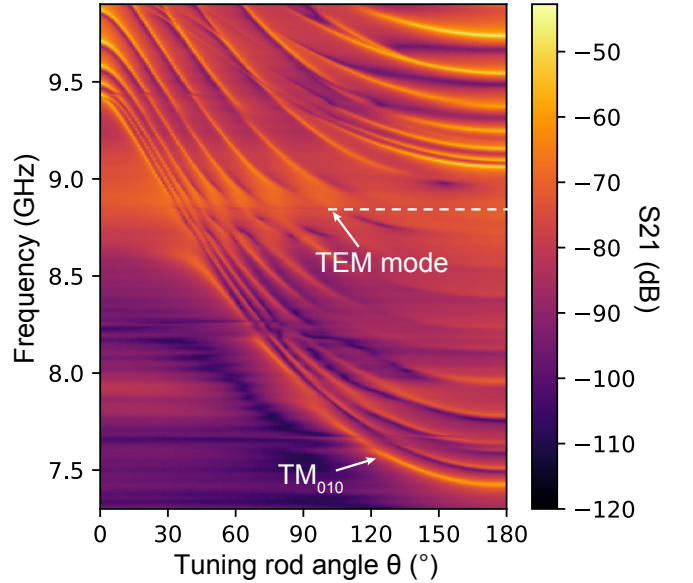


FIG. 5. Mode map for the tuning range of the original 4 row PBG configuration. The color scale represents S_{21} through the PBG, with modes visible as peaks. The TM_{010} mode and an example TEM mode are highlighted. Several higher order TM modes which tune with the TM_{010} are shown. The four expected TEM modes are visible when crossing TM modes. One TEM mode is highlighted with a dashed line for visibility. There are several regions visible where the TM_{010} mode was obscured due to limited coupling and Q . No unexpected modes are visible.

V. THREE ROW TEST RESULTS

To provide better mode visibility over the entire range of rod angles and verify there were no unexpected modes, we tested a version of the design with the innermost row of the PBG lattice removed. This three row configuration increased the defect radius, reducing the aspect ratio and improving coupling significantly. The larger defect size shifts the measured tuning range to 5.659–6.567 GHz. This is similar to the simulated tuning range of 5.616–6.548 GHz. The full simulated tuning behavior is shown in Fig. 6.

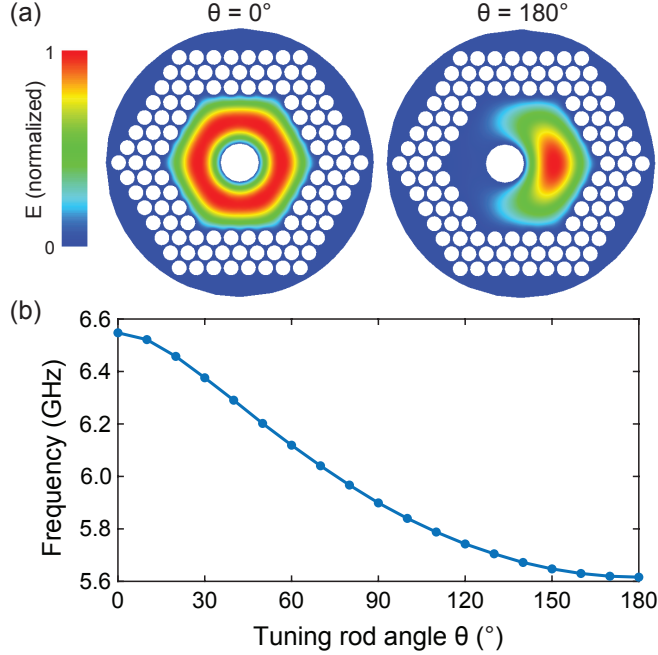


FIG. 6. (a) Normalized magnitude of the electric field in the structure at tuning rod angles of $\theta = 0^\circ$ and 180° . The field at 90° follows the same general shape as the 4 row structure (Fig. 2), but is distorted due to proximity to the TEM mode at 5.9 GHz. The HFSS simulation shown here includes a radiating boundary condition on the outer cylindrical surface. (b) Tuning curve generated from HFSS simulations of the structure including antenna coupling and the alignment grid. Simulations of 10° steps are shown.

We repeated the same procedure used to characterize the four row design, performing bead pull measurements over the full tuning range in 1° steps with multiple antenna couplings. A full mode map is shown in Fig. 7. The expected TEM modes in this region are the 10th and 11th order modes at 5.90 and 6.49 GHz, both of which are visible in the mode map. No unexpected modes were encountered in any part of the tuning range. This determination was made by observing the shape of the mode profile at every tuning angle with several antenna couplings.

Figure 8 shows sample bead perturbation measurements of the TM_{010} without and with mode mixing. In

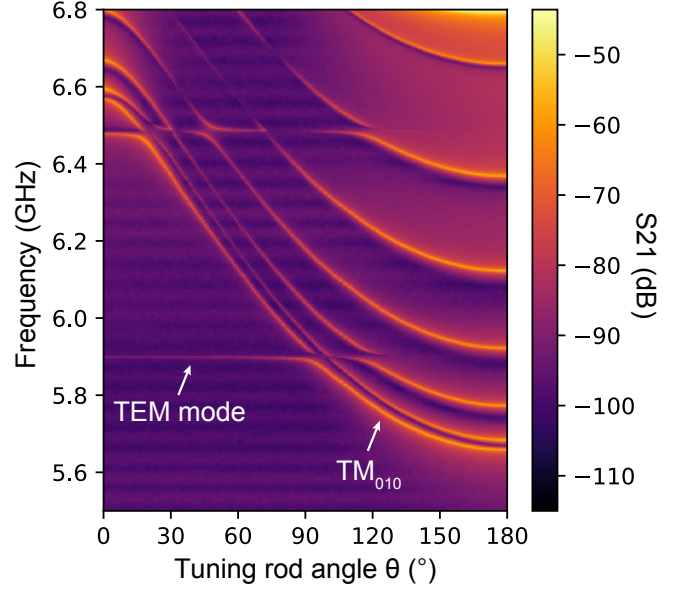


FIG. 7. Mode map for the tuning range of the 3 row PBG configuration. The color scale represents S_{21} through the PBG, with modes visible as peaks. The TM_{010} mode and an example TEM mode are highlighted. There are two TEM modes visible as well as several higher order TM modes which tune with the TM_{010} . The ripple visible at very low S_{21} is likely a standing wave in the measurement network not removed by calibration. This ripple is close to the noise floor of the VNA.

Fig. 7a and b, two typical profiles are shown near the maximum and minimum of the tuning range. The asymmetry of the mode from the bottom to the top of the cavity has been observed in previous cylindrical cavities using this tuning mechanism and changes with rod angle. The impact of this asymmetry on the form factor is negligible [12]. Figure 7c shows an example of the TM_{010} mode mixing with the 10th order TEM mode at 5.90 GHz. The oscillation of the E field of the hybridized mode is clearly visible.

VI. SUMMARY AND FUTURE WORK

We have performed a thorough study of the tuning performance of a tunable PBG resonator, designed to support TM modes and eliminate TE modes. The tuning mechanism and overall structure size were chosen to be compatible with current haloscope techniques. We have successfully demonstrated the elimination of all TE modes, even with a large symmetry-breaking perturbation in the form of a single tuning rod. We have also demonstrated the robustness of the PBG design, showing that even 3 rows of the PBG lattice provides sufficient confinement of the TM_{010} mode to see tuning over the full angle range.

The Q value of this cavity is limited to $\approx 5 \times 10^3$ and does not achieve simulated room temperature values

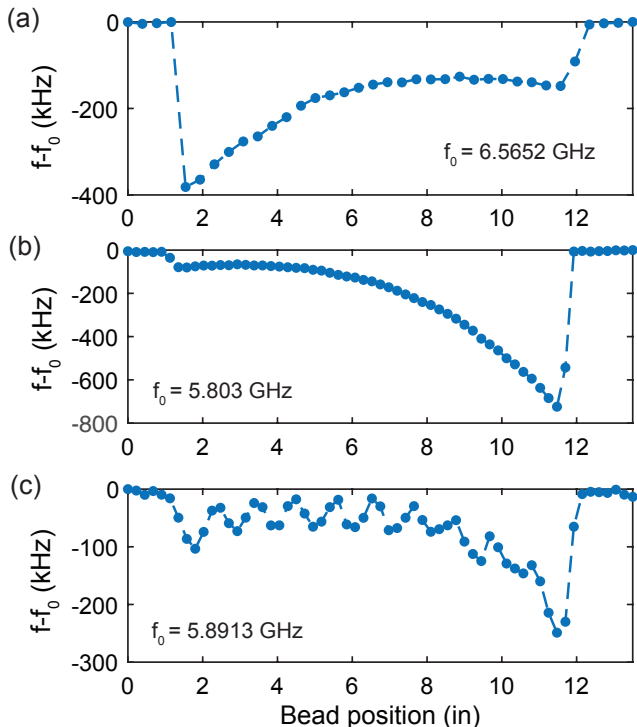


FIG. 8. Sample bead pull measurements of the TM_{010} mode at multiple rod angles: (a) near the maximum of the tuning range, (b) near the minimum of the tuning range, and (c) in the mode crossing with the 10th order TEM mode. The asymmetry of the profile is indicative of axial mode localization, which occurs also in cylindrical cavities with large tuning rods. This asymmetry does not significantly affect the form factor [12].

of $\sim 10^4$. The primary reason for this is poor electrical contact between the rods and the endcaps due to the rod-in-pocket design. Future iterations of PBG structures will explore different fabrication methods to improve the Q value to achieve at least parity with current copper cavities, such as screwing or brazing all lattice rods to the endcaps. As a design created to demonstrate the concept of a tunable PBG, the Q value was not a performance metric and emphasis was placed on ease of fabrication rather than Q value optimization.

A PBG lattice boundary is compatible with other next-generation cavity innovations for axion searches. With this successful demonstration of PBG behavior and the flexibility of the design, ongoing experiments are being performed to explore multi-rod tuning designs and the use of a PBG lattice around a metamaterial resonator, both of which are aimed at reaching higher frequencies. Further work will be performed to explore other materials and the use of higher order modes to improve Q values and reach higher frequencies while maintaining large cavity volumes.

VII. ACKNOWLEDGEMENTS

The authors thank Nolan Kowitt and S. Al Kenany for their work on the bead pull test stand development, and AJ Gubser for the test stand photos. The authors also thank Sergio Velazquez and Amara Johnson for their work fabricating the copper structure. The authors gratefully acknowledge support from the National Science Foundation under Grant No. PHY-2209556. M.C.B. gratefully acknowledges support from the Ronald E. McNair Scholars Program and the Semiconductor Research Corporation.

-
- [1] R. D. Peccei and H. R. Quinn, Constraints imposed by CP conservation in the presence of pseudoparticles, *Phys. Rev. D* **16**, 1791 (1977).
 - [2] R. D. Peccei and H. R. Quinn, CP conservation in the presence of pseudoparticles, *Phys. Rev. Lett.* **38**, 1440 (1977).
 - [3] F. Wilczek, Problem of strong p and t invariance in the presence of instantons, *Phys. Rev. Lett.* **40**, 279 (1978).
 - [4] S. Weinberg, A new light boson?, *Phys. Rev. Lett.* **40**, 223 (1978).
 - [5] J. Preskill, M. B. Wise, and F. Wilczek, Cosmology of the invisible axion, *Physics Letters B* **120**, 127 (1983).
 - [6] F. Chadha-Day, J. Ellis, and D. J. E. Marsh, Axion dark matter: What is it and why now?, *Science Advances* **8**, eabj3618 (2022).
 - [7] P. Sikivie, Experimental tests of the "invisible" axion, *Phys. Rev. Lett.* **51**, 1415 (1983).
 - [8] P. W. Graham, I. G. Irastorza, S. K. Lamoreaux, A. Lindner, and K. A. van Bibber, Experimental searches for the axion and axion-like particles, *Annual Review of Nuclear and Particle Science* **65**, 485 (2015).
 - [9] P. Carenza, T. Fischer, M. Giannotti, G. Guo, G. Martínez-Pinedo, and A. Mirizzi, Improved axion emissivity from a supernova via nucleon-nucleon bremsstrahlung, *JCAP* **10** (10), 016, [Erratum: *JCAP* **05**, E01 (2020)], arXiv:1906.11844 [hep-ph].
 - [10] C. B. Adams *et al.*, Axion Dark Matter, in *Snowmass 2021* (2022) arXiv:2203.14923 [hep-ex].
 - [11] C. O'Hare, cajohare/AxionLimits: AxionLimits, <https://cajohare.github.io/AxionLimits/> (2020).
 - [12] N. M. Rapidis, S. M. Lewis, and K. A. van Bibber, Characterization of the HAYSTAC axion dark matter search cavity using microwave measurement and simulation techniques, *Review of Scientific Instruments* **90**, 024706 (2019).
 - [13] C. Bartram, T. Braine, R. Cervantes, N. Crisosto, N. Du, G. Leum, L. J. Rosenberg, G. Rybka, J. Yang, D. Bowring, A. S. Chou, R. Khatiwada, A. Sonnenschein, W. Wester, G. Carosi, N. Woollett, L. D. Duffy, M. Goryachev, B. McAllister, M. E. Tobar, C. Boutan, M. Jones, B. H. LaRoque, N. S. Oblath, M. S. Taubman, J. Clarke, A. Dove, A. Eddins, S. R. O'Kelley, S. Nawaz, I. Siddiqi, N. Stevenson, A. Agrawal, A. V. Dixit, J. R. Gleason

- son, S. Jois, P. Sikivie, J. A. Solomon, N. S. Sullivan, D. B. Tanner, E. Lentz, E. J. Daw, M. G. Perry, J. H. Buckley, P. M. Harrington, E. A. Henriksen, and K. W. Murch (ADMX Collaboration), Axion dark matter experiment: Run 1b analysis details, *Phys. Rev. D* **103**, 032002 (2021).
- [14] L. Zhong, S. Al Kenany, K. M. Backes, B. M. Brubaker, S. B. Cahn, G. Carosi, Y. V. Gurevich, W. F. Kindel, S. K. Lamoreaux, K. W. Lehnert, S. M. Lewis, M. Malnou, R. H. Maruyama, D. A. Palken, N. M. Rapidis, J. R. Root, M. Simanovskaia, T. M. Shokair, D. H. Speller, I. Urdinarian, and K. A. van Bibber, Results from phase 1 of the HAYSTAC microwave cavity axion experiment, *Phys. Rev. D* **97**, 092001 (2018).
- [15] O. Kwon, D. Lee, W. Chung, D. Ahn, H. Byun, F. Caspers, H. Choi, J. Choi, Y. Chong, H. Jeong, J. Jeong, J. E. Kim, J. Kim, i. m. c. b. u. Kutlu, J. Lee, M. Lee, S. Lee, A. Matlashov, S. Oh, S. Park, S. Uchaikin, S. Youn, and Y. K. Semertzidis, First results from an axion haloscope at CAPP around $10.7 \mu\text{eV}$, *Phys. Rev. Lett.* **126**, 191802 (2021).
- [16] D. Alesini, C. Braggio, G. Carugno, N. Crescini, D. D'Agostino, D. Di Gioacchino, R. Di Vora, P. Falferi, U. Gambardella, C. Gatti, G. Iannone, C. Ligi, A. Lombardi, G. Maccarrone, A. Ortolan, R. Pengo, C. Pira, A. Rettaroli, G. Ruoso, L. Taffarello, and S. Tocci, High quality factor photonic cavity for dark matter axion searches, *Review of Scientific Instruments* **91**, 094701 (2020).
- [17] M. Simanovskaia, A. Droster, H. Jackson, I. Urdinarian, and K. van Bibber, A symmetric multi-rod tunable microwave cavity for a microwave cavity dark matter axion search, *Review of Scientific Instruments* **92**, 033305 (2021).
- [18] E. Yablonovitch, Photonic band-gap structures, *J. Opt. Soc. Am. B* **10**, 283 (1993).
- [19] E. Yablonovitch, Photonic band structure, in *Analogies in Optics and Micro Electronics: Selected Contributions on Recent Developments*, edited by W. van Haeringen and D. Lenstra (Springer Netherlands, Dordrecht, 1990) pp. 117–133.
- [20] E. I. Smirnova, C. Chen, M. A. Shapiro, J. R. Sirigiri, and R. J. Temkin, Simulation of photonic band gaps in metal rod lattices for microwave applications, *Journal of Applied Physics* **91**, 960 (2002).
- [21] E. I. Smirnova, *Novel photonic band gap structures for accelerator applications*, Ph.D. thesis, Massachusetts Institute of Technology (2005).
- [22] B. J. Munroe, J. Zhang, H. Xu, M. A. Shapiro, and R. J. Temkin, Experimental high gradient testing of a 17.1 GHz photonic band-gap accelerator structure, *Phys. Rev. Accel. Beams* **19**, 031301 (2016).
- [23] E. I. Simakov, S. A. Arsenyev, C. E. Buechler, R. Edwards, and W. Romero, Experimental study of wakefields in an X-band photonic band gap accelerating structure, *AIP Conference Proceedings* **1777**, 060011 (2016).
- [24] J. R. Sirigiri, K. E. Kreischer, J. Machuzak, I. Mastovsky, M. A. Shapiro, and R. J. Temkin, Photonic-band-gap resonator gyrotron, *Phys. Rev. Lett.* **86**, 5628 (2001).
- [25] J. Zhang, B. J. Munroe, H. Xu, M. A. Shapiro, and R. J. Temkin, High power experimental studies of hybrid photonic band gap accelerator structures, *Phys. Rev. Accel. Beams* **19**, 081304 (2016).
- [26] E. A. Nanni, S. M. Lewis, M. A. Shapiro, R. G. Griffin, and R. J. Temkin, Photonic-band-gap traveling-wave gyrotron amplifier, *Phys. Rev. Lett.* **111**, 235101 (2013).
- [27] S. Arsenyev, C. Boulware, T. Grimm, A. Rogacki, D. Shchegolkov, and E. Simakov, Five-cell Superconducting RF Module with a PBG Coupler Cell: Design and Cold Testing of the Copper Prototype, in *Proc. 6th International Particle Accelerator Conference (IPAC'15), Richmond, VA, USA, May 3-8, 2015*, International Particle Accelerator Conference No. 6 (JACoW, Geneva, Switzerland, 2015) pp. 3475–3478.
- [28] Dassault Systèmes, CST Studio Suite, <https://www.3ds.com/products/simulia/cst-studio-suite>.
- [29] Ansys, Ansys HFSS: 3D High Frequency Simulation Software, <https://www.ansys.com/products/electronics/ansys-hfss>.
- [30] L. C. Maier and J. C. Slater, Field strength measurements in resonant cavities, *Journal of Applied Physics* **23**, 68 (1952).
- [31] S. M. Hanna, G. B. Bowden, H. A. Hoag, R. Loewen, A. E. Vlieks, and J. W. Wang, A semi-automated system for the characterization of nlc accelerating structures, in *Proceedings Particle Accelerator Conference*, Vol. 2 (1995) pp. 1108–1110 vol.2.
- [32] S. A. Kenany, M. Anil, K. Backes, B. Brubaker, S. Cahn, G. Carosi, Y. Gurevich, W. Kindel, S. Lamoreaux, K. Lehnert, S. Lewis, M. Malnou, D. Palken, N. Rapidis, J. Root, M. Simanovskaia, T. Shokair, I. Urdinarian, K. van Bibber, and L. Zhong, Design and operational experience of a microwave cavity axion detector for the 20–100 μeV range, *Nuclear Instruments and Methods in Physics Research Section A: Accelerators, Spectrometers, Detectors and Associated Equipment* **854**, 11 (2017).